GSA DATA REPOSITORY 2015273

SUPPLEMENTAL MATERIAL

EBSD data collection details

Crystallographic orientations were collected by means of electron backscatter diffraction (EBSD) analysis on oriented sections cut parallel to the *XZ* plane of the fabric (*X* parallel to mineral stretching lineation, *Z* normal to foliation plane). EBSD data were acquired within the Department of Earth and Environmental Sciences at Boston College on a Tescan Mira 3 LMU Schottky field emission scanning electron microscope equipped with an Oxford Instruments Nordyls Max2 EBSD detector.

Acquisition settings utilized an accelerating voltage of 25 kV and beam currents ranging from 40-70 nA. Crystallographic orientation maps were acquired using version 3.0 of Oxford Instruments AZtecHKL acquisition and analysis software. Electron backscatter patterns were indexed using 2x2 camera binning (320x240 pixels), a Hough resolution of 100, and center detection of 12 bands using the 'refined accuracy' mode. Since meaningful application of CVA analysis requires orientation maps be acquired at sufficient resolution as to yield multiple orientation solutions per grain, step sizes of 2, 3.5, and 7.5 μm were used for map regions in samples GLSZ-18, SL-25-02, and 12NB114 respectively. EBSD datasets correspondingly comprise 4-9 million individual crystallographic solutions, ensuring multiple intragranular crystallographic solutions across the full range of grain sizes within a sample.

Crystallographic orientation maps were processed using the open source software toolbox *MTEX* (v3.5) for *Matlab*® (Mathworks, Natick, MA, USA). Grain sets used in the CVA analysis were constructed using misorientation boundaries of ≥10º (Bachmann et al., 2011). Non-indexed phases were retained in the dataset to avoid artificially 'filling' orientations within grain sets. Axial plots of crystallographic data are shown in Supplementary Figure 3.

Crystallographic vorticity analysis

For mathematical analysis, crystallographic orientations measured by EBSD are expressed using three mutually perpendicular unit vectors in right-handed order. Orthonormal vectors are chosen that point along the principal axes of each crystallographic unit cell (i.e., equivalent to Miller indices [100], [010], [001]). Once coordinates are chosen on the ambient space, each of these vectors is expressible as a list of three numbers. The vectors are placed into the rows of a 3x3 matrix **R**, which is then special orthogonal. Geometrically, this matrix represents the rotation that reorients the three vectors into alignment with the three coordinate axes of the ambient space.

The rotation matrix **R** is defined only up to the crystallographic point group of the mineral. For example, this paper's applications deal with alpha-quartz, which has a trigonal trapezohedral point group. Let **I** be the 3x3 identity tensor, let

$$\mathbf{J} = \begin{bmatrix} \cos(2\,\pi\,/\,3) & -\sin(2\,\pi\,/\,3) & 0 \\ \sin(2\,\pi\,/\,3) & \cos(2\,\pi\,/\,3) & 0 \\ 0 & 0 & 1 \end{bmatrix}$$

be rotation about the z-axis of space through 2 π / 3 = 120 degrees, and let

$$\mathbf{K} = \begin{bmatrix} 1 & 0 & 0 \\ 0 & -1 & 0 \\ 0 & 0 & -1 \end{bmatrix}$$

be rotation about the x-axis through π = 180 degrees. Then the trigonal trapezohedral point group is $\mathbf{G} = \{\mathbf{I}, \mathbf{J}, \mathbf{J}^2, \mathbf{K}, \mathbf{J}\,\mathbf{K}\,\mathbf{J}^2, \mathbf{J}^2\mathbf{K}\,\mathbf{J}\}$. For any rotation $\mathbf{Q}$ in $\mathbf{G}$, the rotation $\mathbf{Q}\,\mathbf{R}$ represents the crystal orientation equally as well as $\mathbf{R}$ does. In other words, the datum $\mathbf{R}$ is actually a set

$$\mathbf{G}\,\mathbf{R} = \{\mathbf{I}, \mathbf{J}, \mathbf{J}^2, \mathbf{K}, \mathbf{J}\,\mathbf{K}\,\mathbf{J}^2, \mathbf{J}^2\mathbf{K}\,\mathbf{J}\}\mathbf{R} = \{\mathbf{R}, \mathbf{J}\,\mathbf{R}, \mathbf{J}^2\mathbf{R}, \mathbf{K}\,\mathbf{R}, \mathbf{J}\,\mathbf{K}\,\mathbf{J}^2\mathbf{R}, \mathbf{J}^2\mathbf{K}\,\mathbf{J}\,\mathbf{R}\}$$

of six rotations. There is no physical reason to prefer one of these six representative rotations over the others. This ambiguity complicates some calculations with orientational data, especially when they are not highly concentrated.

Almost all of our intragranular data sets are highly concentrated, as is typical of EBSD data (Bachmann et al., 2010). One simple measure of concentration is orientation diameter: the maximum distance between any two orientations in the data set (The distance between two orientations is the minimum distance between their representative rotations. The distance between two rotations $\mathbf{R}_i$ and $\mathbf{R}_j$ in the space SO(3) of rotations is the angle of the rotation $\mathbf{R}_i\mathbf{R}_j^{\mathrm{T}}$). The GLSZ data set comprises 60,828 grains, whose orientation diameters are all less than π / 3 (quartiles: 0.0054, 0.0298, 0.0602, 0.1344, 0.8586). The WISZ data set comprises 1,213 grains with orientation diameters all less than π / 3 (quartiles: 0.0124, 0.0644, 0.1047, 0.1642, 0.5304). The MTZ data set comprises 74,724 grains, all but 51 of which (0.07%) have orientation diameters less than π / 3 (quartiles: 0.0070, 0.0756, 0.1311, 0.2005, 1.7236). Therefore, except for a few unusual grains from MTZ, each of our grains has this property: Representative rotations $\{\mathbf{R}_1, \ldots, \mathbf{R}_n\}$ can be chosen for the *n* orientations in the grain, such that all $\mathbf{R}_i$ are within a distance of π / 3 from each other.

Working within a single grain, let $\overline{\mathbf{R}}$ be the Fréchet mean rotation of the $\mathbf{R}_i$ (e.g., Krakowski et al., 2007; Hartley et al., 2013). Because all of the $\mathbf{R}_i$ are within distance π / 3 from each other, computation of $\overline{\mathbf{R}}$ is guaranteed to converge, and the $\mathbf{R}_i$ are also less than distance π / 3 from $\overline{\mathbf{R}}$. Each $\mathbf{R}_i$ is the representative of its datum $\mathbf{G}\mathbf{R}_i$ that is closest to $\overline{\mathbf{R}}$. For if there were another closer representative, say $\mathbf{Q}\,\mathbf{R}_i$ with $\mathbf{Q} \neq \mathbf{I}$, then the distance from $\mathbf{R}_i$ to $\mathbf{Q}\,\mathbf{R}_i$ would be less than 2 π / 3 by the triangle inequality. But the distance from $\mathbf{R}_i$ to $\mathbf{Q}\,\mathbf{R}_i$ equals the distance from $\mathbf{I}$ to $\mathbf{Q}$, which is at least 2 π / 3 for any $\mathbf{Q} \neq \mathbf{I}$ in the trigonal trapezohedral group $\mathbf{G}$.

We proceed by principal geodesic analysis (Fletcher et al., 2004). This method uses only the data representatives nearest to $\overline{\mathbf{R}}$, which are the $\mathbf{R}_i$ by the argument above. The method approximates the space SO(3) of rotations by its tangent space at the mean $\overline{\mathbf{R}}$, which is a three-dimensional vector space. The method transfers each datum $\mathbf{R}$ into that vector space and performs principal components analysis on the resulting vectors. The first principal component amounts to the line through the vector data that minimizes the sum of squared perpendicular distances from the vectors to the line. Transferring the line back to SO(3) produces a geodesic curve that approximately best-fits the data $\{\mathbf{R}_1, \ldots, \mathbf{R}_n\}$ (e.g., Fig. 1, Supp. Fig. 4), in that it approximately minimizes the sum of squared distances from the $\mathbf{R}_i$ to the curve. A parameterization of this curve is

$$\mathbf{R}(t) = \overline{\mathbf{R}}\mathbf{Q}(t),$$

where

$$\mathbf{Q}(t) = \mathbf{I} + (\sin t)\mathbf{U} + (\mathbf{1} - \cos t)\mathbf{U}^{\mathbf{2}},$$

$$\mathbf{U} = \begin{bmatrix} 0 & -u_3 & u_2 \\ u_3 & 0 & -u_1 \\ -u_2 & u_1 & 0 \end{bmatrix},$$

and

$$\mathbf{u} = [u_1 \ u_2 \ u_3]^{\mathrm{T}}$$

is a unit vector. Computationally, $\mathbf{u}$ is the first principal component described earlier. Geometrically, $\mathbf{u}$ is the axis, about which $\mathbf{Q}(t)$ is a steady rotation.

As t varies, the three rows of $\mathbf{R}(t)$ trace out three curves on the unit sphere. The vector $\mathbf{R}(t)\mathbf{u}$ consists of three numbers, which are the dot products of the three rows of $\mathbf{R}(t)$ with $\mathbf{u}$. Notice that $\mathbf{U}\mathbf{u} = 0$, and thus $\mathbf{R}(t)\mathbf{u} = \overline{\mathbf{R}}\mathbf{u}$ for all t. Therefore all three dot products are constant with respect to t, and so the three curves on the unit sphere are arcs of small circles about the pole $\mathbf{u}$. In this way, $\mathbf{u}$ is the approximate best-fit dispersion pole for the three perpendicular crystallographic axes simultaneously.

Such grain-scale crystallographic dispersion poles can be computed for each grain separately in a sample to assemble a representative group of intragranular vorticity axes. We identify the vector coordinates of a preferred dispersion/vorticity axis using non-parametric kernel density estimation (de la Vallée Poussin kernel) applied to the set of intragranular dispersion axes. The preferred crystallographic dispersion axis is considered to approximate the bulk sample-scale vorticity axis.

Access to code for CVA analysis

The CVA analysis outlined in this paper was implemented using our own custom code in combination with the free and open source software toolbox *MTEX* (v3.5 and v4.0) for *Matlab*® (Mathworks, Natick, MA, USA). Currently, there is no option for conducting CVA analysis using commercial EBSD software. However, our code is freely available for download (https://github.com/zmichels/CVA) or by email request from the corresponding author, Z.

Michels (zmichels@wisc.edu). Readers are also encouraged to contact Z. Michels with any questions regarding code usage or customization.

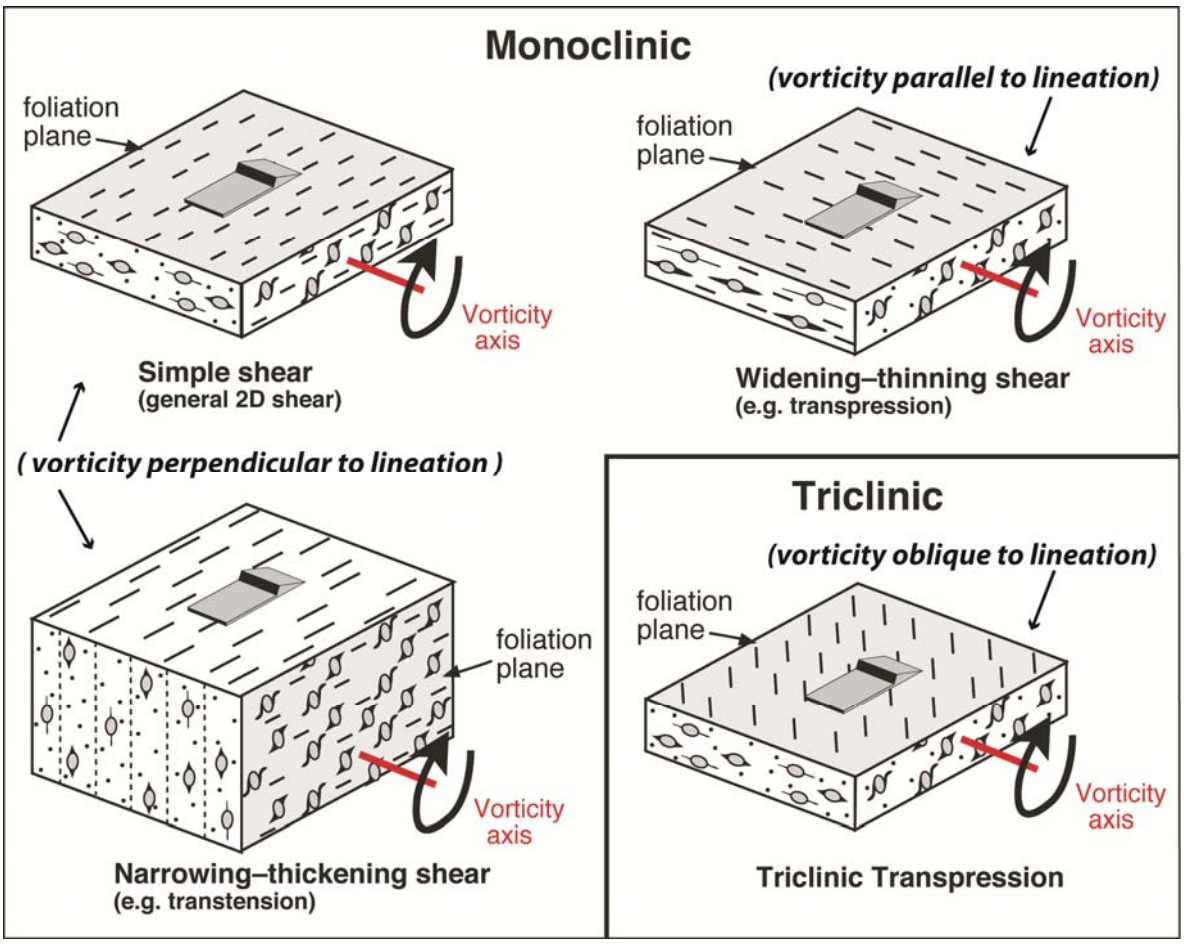

Figure DR1. Relationships between vorticity, fabric elements, and shear sense indicators within various types of shear zones (Modified after Tikoff et al., 2013). Vorticity axes are expressed in the rock fabric as the pole to a surface that contains the best-developed and most-consistent sense-of-shear indicators. Simple shear zones contain vorticity axes that lie within the plane of foliation, perpendicular to the lineation. Kinematic models of deformations that deviate from simple shear suggest the occurrence of other possibilities, including vorticity axes that are parallel to lineation (e.g., transpression), perpendicular to the foliation (e.g., transtension), and oblique to both lineation and foliation (e.g., triclinic transpression). Patterns predicted by transpression and triclinic transpression have been found in natural shear zones.

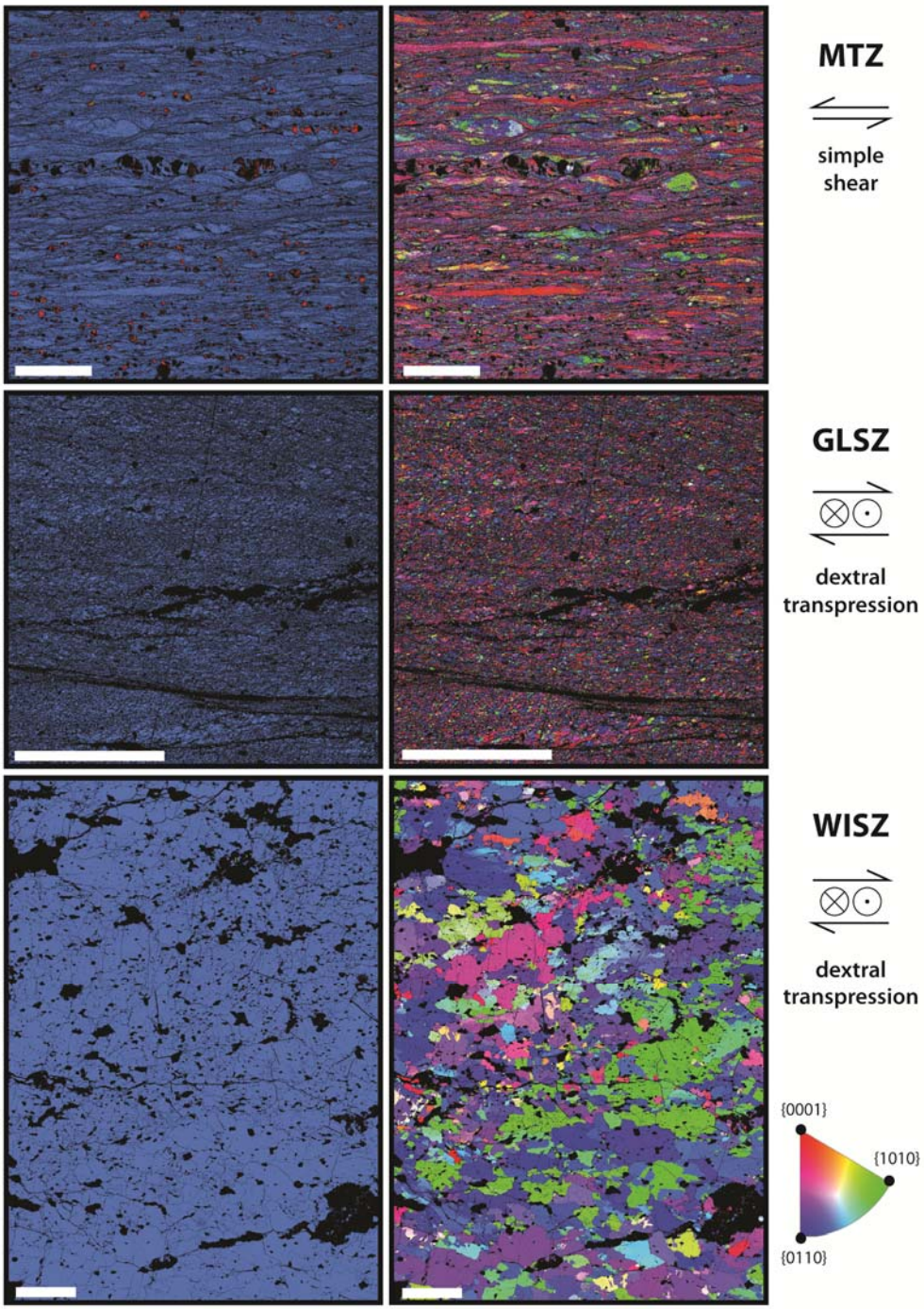

Figure DR2. EBSD maps of quartzite samples from three different shear zone localities (MTZ = Moine Thrust Zone, GLSZ = Gem Lake Shear Zone, WISZ = Western Idaho Shear Zone). Maps on the left are colored by phase (blue = quartz, red = anorthite, black = not indexed). Maps on the right are color coded using the inverse pole figure color wedge shown to indicate crystallographic orientation relative to the map *z*-direction (out of the page). All maps are parallel to macroscopic lineation (map *x*-direction) and perpendicular to foliation (map *y*-direction). White scale bar is 2mm.

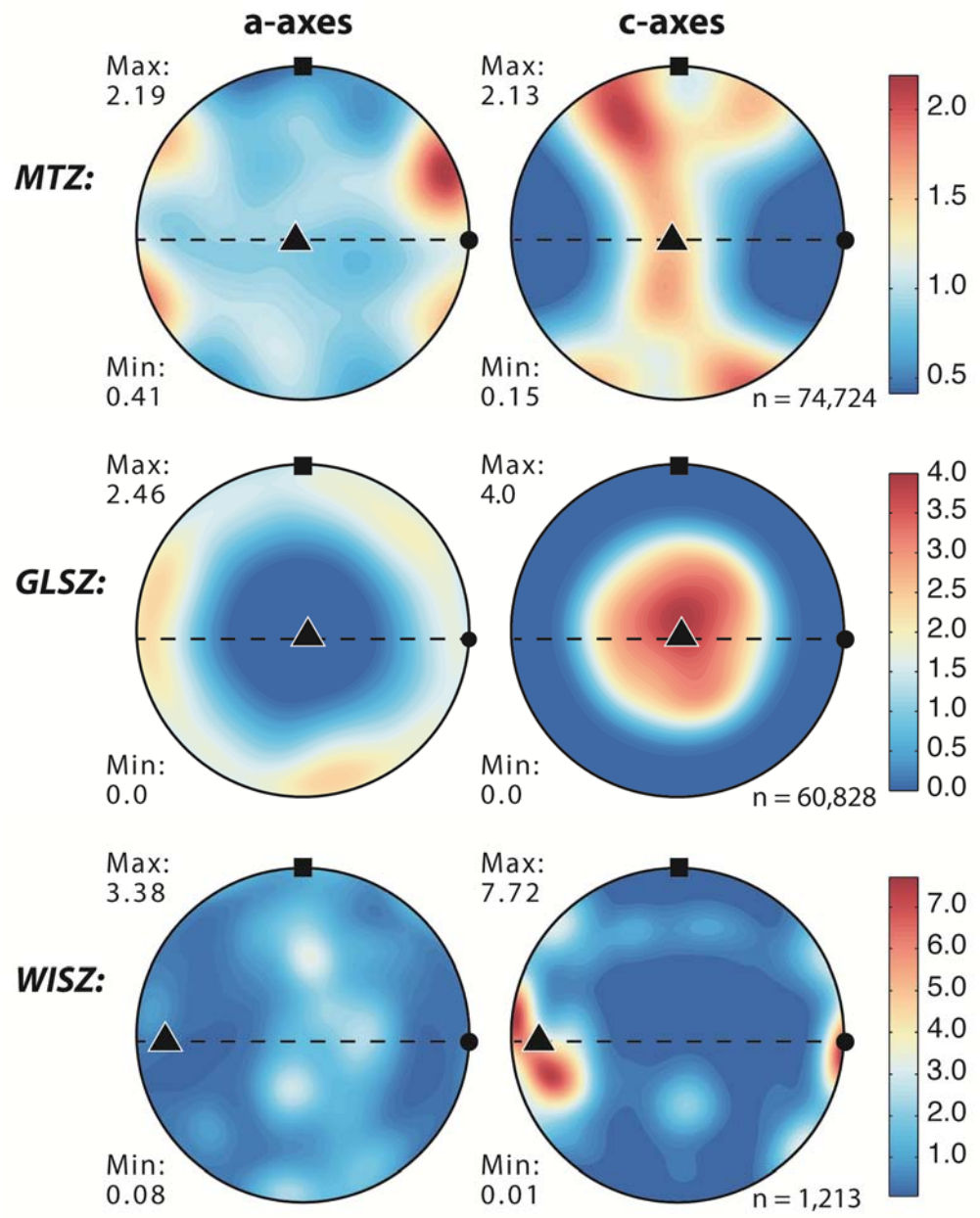

Figure DR3. Contoured lower hemisphere equal area projections of quartz a- and c-axes (MTZ = Moine Thrust Zone; GLSZ = Gem Lake Shear Zone; WISZ = Western Idaho Shear Zone) and bulk vorticity axes calculated using CVA (black triangles). All plots are shown in the same macroscopic fabric-relative reference frame – analyzed specimen surfaces are parallel to lineation (black dot) and perpendicular to foliation (black square shows pole to foliation, and dashed line shows the foliation trace). Color scales indicate multiples of uniform density of orientation density functions calculated from mean grain orientations (1 point per grain; number of grains indicated for each sample) using a de la Vallée Poussin kernel and a 10º halfwidth.

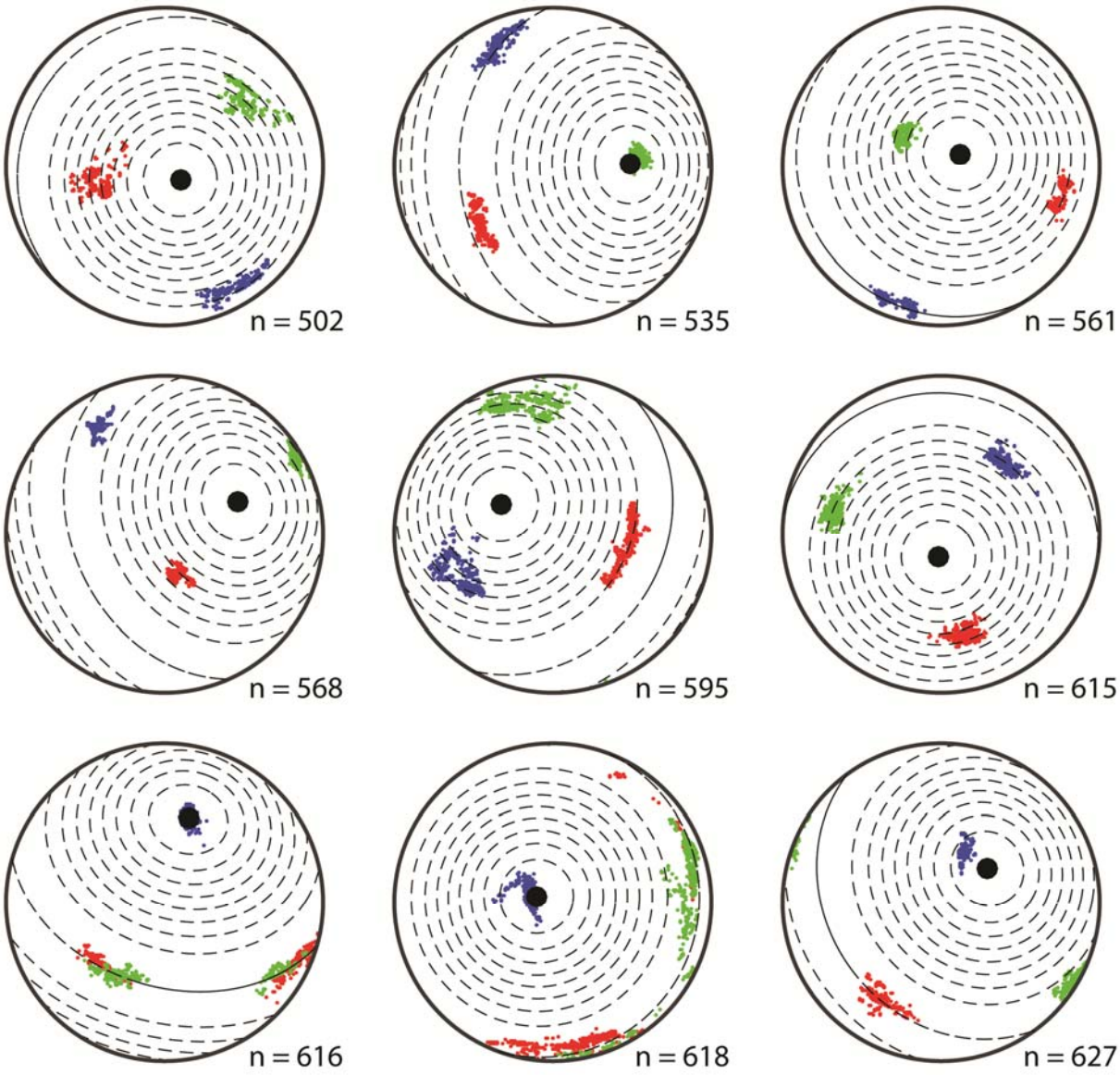

Figure DR4. Additional example results of intragranular CVA analysis applied to individual grains from the Moine thrust zone sample (#SL35-02). Lower hemisphere equal-area projections show the primary intragranular crystallographic axes (i.e., Miller indices [100], [010], and [001]; red, green, and blue dots, respectively) and the dispersion axis calculated using CVA analysis (black dot). Nine grains comprising similar number of orientation solutions (n = 502–627) were randomly selected. Dashed arcs indicate the trace of steady rotations about the calculated dispersion axes to give a visual sense of the goodness of fit.

REFERENCES CITED

Bachmann, F., Hielscher, R., Jupp, P.E., Pantleon, W., Schaeben, H., and Wegert, E., 2010, Inferential statistics of electron backscatter diffraction data from within individual crystalline grains: Journal of Applied Crystallography, v. 43, no. 6, p. 1338–1355, doi:10.1107/S002188981003027X.

Bachmann, F., Hielscher, R., and Schaeben, H., 2011, Grain detection from 2d and 3d EBSD data—Specification of the MTEX algorithm: Ultramicroscopy, v. 111, p. 1720–1733, doi:10.1016/j.ultramic.2011.08.002.

Fletcher, P.T., Lu, C., Pizer, S.M., and Joshi, S., 2004, Principal geodesic analysis for the study of nonlinear statistics of shape: IEEE Transactions on Medical Imaging, v. 23, p. 995–1005, doi:10.1109/TMI.2004.831793.

Hartley, R., Trumpf, J., Dai, Y., and Li, H., 2013, Rotation averaging: International Journal of Computer Vision, v. 103, p. 267–305, doi:10.1007/s11263-012-0601-0.

Krakowski, K.A., Huper, K., and Manton, J.H., 2007, On the computation of the Karcher mean on spheres and special orthogonal groups, in Proceedings of the Workshop on Robotics and Mathematics, RoboMat07, (2007). ISBN: 978-989-95011-3-3.

Tikoff, B., Blenkinsop, T., Kruckenberg, S.C., Morgan, S., Newman, J., and Wojtal, S., 2013, A perspective on the emergence of modern structural geology: Celebrating the feedbacks between historical-based and process-based approaches, in Bickford, M.E., ed., The Web of Geological Sciences: Advances, Impacts, and Interactions: Geological Society of America Special Papers, v. 500, p. 65–119, doi:10.1130/2013.2500(03).